Chaotic pattern transitions in pulse neural networks

Takashi Kanamaru

Department of Innovative Mechanical Engineering,
Faculty of Global Engineering, Kogakuin University,
139 Inume, Hachioji-city, Tokyo 193-0802, Japan

Abstract

In models of associative memory composed of pulse neurons, chaotic pattern transitions where the pattern retrieved by the network changes chaotically were found. The network is composed of multiple modules of pulse neurons, and when the inter-module connection strength decreased, the stability of pattern retrieval changed from stable to chaotic. It was found that the mixed pattern of stored patterns plays an important role in chaotic pattern transitions.

1   Introduction

Chaotic associative memory which incorporates chaotic dynamics into static associative memory, was proposed by several researchers in the 1990s (Adachi & Aihara, 1997; Aihara, Takabe, & Toyoda, 1990; Inoue & Nagayoshi, 1991; Nara & Davis, 1992; Tsuda, 1992; Uchiyama & Fujisaka, 2004). In such models, the pattern retrieved by the network changes chaotically, and such phenomena are thought to be related to chaotic itinerancy in high-dimensional dynamical systems (Kaneko & Tsuda, 2000). Previous models of chaotic associative memory were composed of conventional analog-valued models of neurons. However, considering the actual brain, chaotic associative memory should be modeled using pulse neural networks (PNNs) which are thought to be more precise than networks of analog-valued neurons.

Many studies demonstrated chaotic dynamics in models of single pulse neurons (Feudel et al., 2000; Varona et al., 2001) and in PNNs (Kanamaru, 2006; Kanamaru & Sekine, 2005; Torikai & Saito, 2004; Tsumoto, Yoshinaga, & Kawakami, 2002; van Vreeswijk & Sompolinsky, 1996; Yoshioka, 2005). However, to our knowledge, there has been no study on chaotic associative memory using PNNs, and this may be because of the following reasons: it is unclear whether the chaos in models of associative memory is generated by single neurons or by neural networks; the range of values of parameters where chaos exists in a pulse neuron is often narrow, namely, chaos in a pulse neuron can easily be broken by noise; chaos caused by neural networks is often high-dimensional, and

its analysis is difficult.

In the present study, we could construct PNNs that show properties of chaotic associative memory. This paper is organized as follows. In Section 2, a pulse neural network composed of class 1 excitable neurons with excitatory and inhibitory connections is defined, and synchronized chaotic firings are found in the network. In the subsequent sections, this network is called the one-module system, and it is used as one element of the usual model of associative memory. In other words, in our model, chaos is generated by the interactions of the network, but, when viewed as a model of associative memory, chaos is generated in an element of the network. In Section 3, we construct a model of associative memory using a network of multiple modules, and we found chaotic pattern transitions in this network. A similar phenomenon was observed in a network composed of a finite number of Morris-Lecar neurons. In Section 4, the properties of chaotic pattern retrieval are examined. It was found that the mixed pattern of stored patterns plays an important role in chaotic pattern transitions. It was also found that several instabilities exist even when memory retrieval is stable. The final section provides a discussion and conclusions.

2   One-module system

Let us define a pulse neural network composed of N_E excitatory neurons and N_I inhibitory neurons with internal states $\theta_E^{(i)}$ and $\theta_I^{(i)}$, respectively, that are written as

$$
\begin{aligned}
\dot{\theta}_E^{(i)} &= (1 - \cos\theta_E^{(i)}) + (1 + \cos\theta_E^{(i)}) \\
&\quad \times (r_E + \xi_E^{(i)}(t) + g_{EE}I_E(t) - g_{EI}I_I(t)), \quad (1)
\end{aligned}
$$

$$
\begin{aligned}
\dot{\theta}_I^{(i)} &= (1 - \cos\theta_I^{(i)}) + (1 + \cos\theta_I^{(i)}) \\
&\quad \times (r_I + \xi_I^{(i)}(t) + g_{IE}I_E(t) - g_{II}I_I(t)), \quad (2)
\end{aligned}
$$

$$
I_X(t) = \frac{1}{2N_X} \sum_{j=1}^{N_X} \sum_{k} \frac{1}{\kappa_X} \exp\left(-\frac{t - t_k^{(j)}}{\kappa_X}\right), \quad (3)
$$

$$
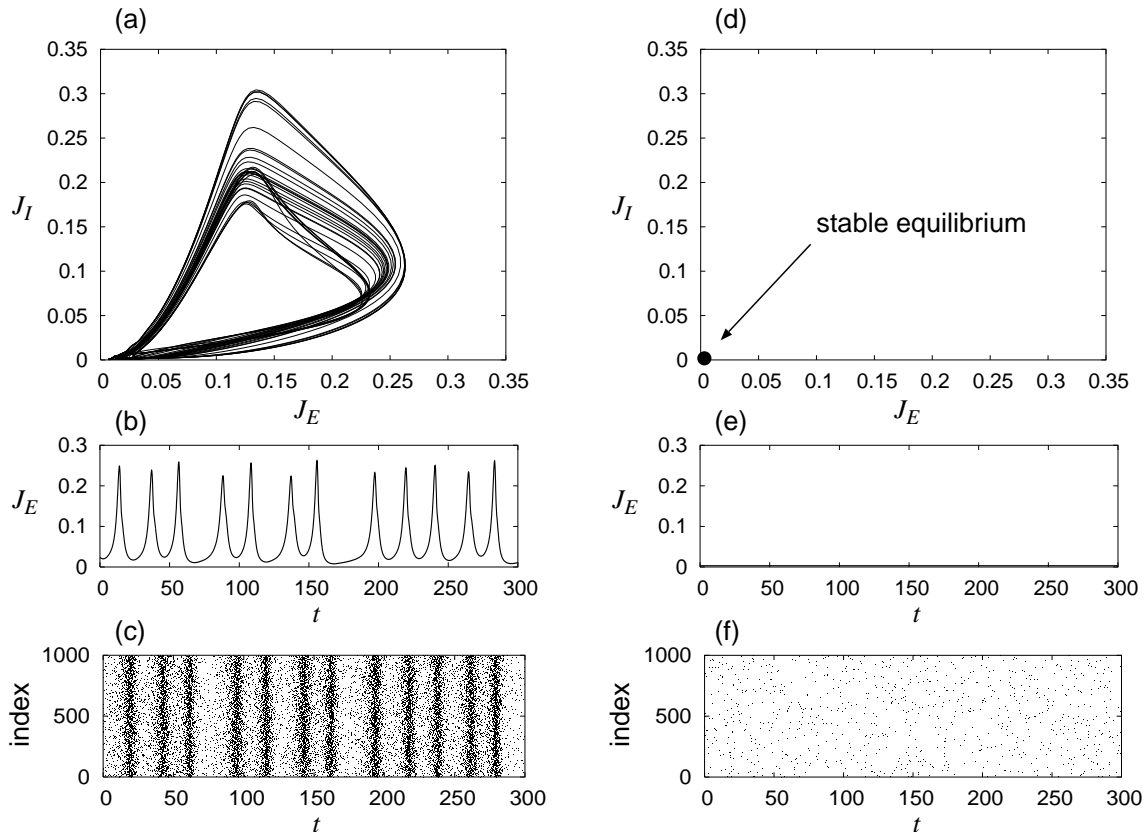\langle \xi_X^{(i)}(t)\xi_Y^{(j)}(t') \rangle = D\delta_{XY}\delta_{ij}\delta(t - t'), \quad (4)
$$

Figure 1: (a), (b), and (c) Synchronized chaotic firings of neurons for $r_E = r_I = -0.025$, $D = 0.0032$, $g_{int} = 4$, and $g_{ext} = 2.5$. (a) A trajectory of the instantaneous firing rates J_E and J_I. (b) Change in J_E over time. (c) A raster plot of the firing times of the excitatory neurons in the network with $N_E = N_I = 1000$. (d), (e), and (f) Asynchronous firings that coexist with synchronized chaotic firings. Although the values of the parameters are identical with those of (a), (b), and (c), the system converges to this asynchronous state due to different initial conditions.

where X and Y each denote the excitatory ensemble E or the inhibitory ensemble I, $t_k^{(j)}$ is the k-th firing time of the j-th neuron in ensemble X, and the firing time is defined as the time at which $\theta_X^{(j)}$ exceeds π in the positive direction. $I_X(t)$ is the sum of synaptic inputs from the neurons in ensemble X, and the form of the post-synaptic potential is an exponential function. r_X denotes the parameters of the neurons in ensemble X, g_{XY} denotes the connection strength from ensemble Y to X, $\xi_X^{(i)}(t)$ denotes noise in the i-th neuron in ensemble X, and it can be interpreted as the sum of synaptic inputs from neurons that belong to other external networks. Note that the model of neurons with $\dot{\theta} = (1 - \cos\theta) + (1 + \cos\theta)r$ is the canonical model of class 1 neurons that is also known as the theta model (Ermentrout, 1996; Ermentrout & Kopell, 1986; Gutkin & Ermentrout, 1998), and it is known that arbitrary class 1 neurons near their bifurcation points can be transformed into the canonical model. Application of the canonical model was previously extended to slowly connected class 1 networks (Izhikevich, 1999, 2000), and the sys-

tem governed by Eqs. (1), (2), and (3) has this form. Therefore, arbitrary networks of slowly connected class 1 neurons with global connections can be transformed into the above form.

In the absence of synaptic inputs $I_X(t)$ and noise $\xi_X^{(i)}(t)$, a single neuron shows self-oscillation when the system parameter r_X satisfies $r_X > 0$. When $r_X < 0$, this neuron becomes an excitable system with a stable equilibrium written by

$$\theta_0 = -\arccos\frac{1 + r_X}{1 - r_X}, \qquad (5)$$

in which θ_0 is close to zero for $r_X \sim 0$. In the following, we use values of the parameter $r_X < 0$ and we consider the dynamics of networks of excitable neurons. For simplicity, the restrictions, $g_{EE} = g_{II} \equiv g_{int}$ and $g_{EI} = g_{IE} \equiv g_{ext}$, are placed, where g_{int} is the internal connection strength in an ensemble, and g_{ext} is the external connection strength between excitatory and inhibitory ensembles, and the parameters r_E and r_I and the noise intensity D are set as uniform in the network. We call this network composed of excitatory and

2

inhibitory neurons as a one-module system.

As shown in Appendix A, in the limit of $N_E, N_I \to \infty$, the average dynamics of the one-module system can be analyzed using the Fokker-Planck equation (Gerstner & Kistler, 2002; Kuramoto, 1984), and various synchronized firings including chaotic ones were found (Kanamaru, 2006; Kanamaru & Sekine, 2005). A trajectory of instantaneous firing rates J_E and J_I of the excitatory and inhibitory ensembles, respectively, is shown in Fig. 1(a) and the change in J_E over time is shown in Fig. 1(b). Note that J_E and J_I are defined as $J_X \equiv J_X(\pi, t)$ where $J_X(\theta_X, t)$ is the probability flux of ensemble X as shown in Appendix A. In Fig. 1(a), a low-dimensional chaotic attractor is observed, and the largest Lyapunov exponent of this strange attractor was numerically confirmed to be positive (Kanamaru & Sekine, 2005). Although the above results were obtained for a network composed of an infinite number of neurons, similar phenomena can be observed in a network composed of a finite number of neurons as shown in Fig. 1(c), where a raster plot of the firings of the excitatory neurons in a network with $N_E = N_I = 1000$ is shown. To integrate the stochastic differential equations numerically, the second-order Runge-Kutta method (Klauder & Petersen, 1985) was used.

Moreover, a stable equilibrium coexists with the chaotic attractor, and this equilibrium is shown in Figs. 1(d), (e), and (f). It can be observed that the stable equilibrium of the Fokker-Planck equation corresponds to asynchronous firings of neurons in the network of a finite number of neurons. The system converges to either the chaotic attractor or the stable equilibrium depending on the initial conditions. For more information about the bifurcation in this system, please see Kanamaru (2006).

3 Chaotic pattern transitions in the system with multiple modules

In this section, we use the one-module system defined in the previous section as a single element in a model of associative memory, and we demonstrate chaotic pattern transitions in this model.

We consider a network with M modules, each of which is composed of N_E excitatory neurons and N_I inhibitory neurons; namely, there are $(N_E + N_I)M$ neurons in this network. A schematic diagram of the inter-module connections is shown in Fig. 2(a). Although only two modules are shown in this diagram for simplicity, M modules are actually connected. The inter-module connections stem only from the excitatory ensembles, and it is based on the experimental fact that the inter-columnar horizontal connections are excitatory (Gilbert & Wiesel, 1983; Ts'o, Gilbert, & Wiesel, 1986). More specifically, the synaptic input T_{Ei} to the excitatory ensemble in the i-th module and the synaptic input T_{Ii} to the inhibitory
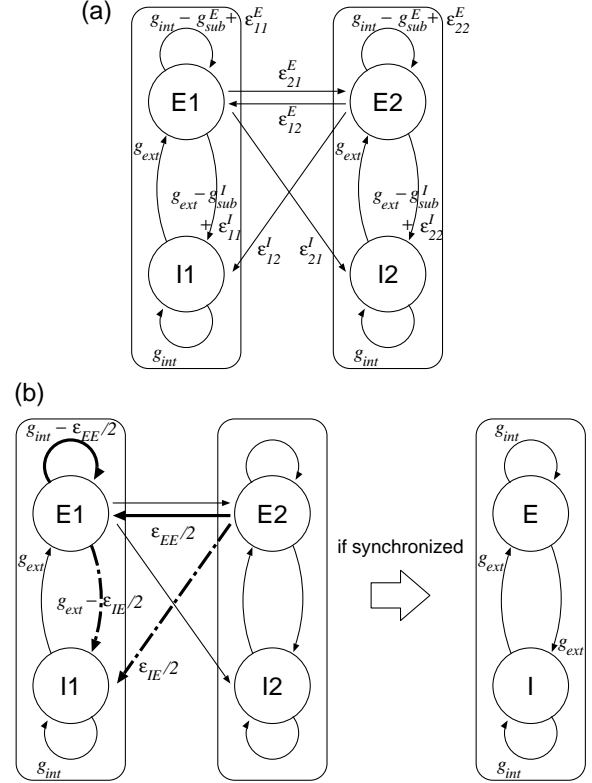

Figure 2: (a) Schematic diagram of the inter-module connections between two modules. The two circles in a module denote excitatory and inhibitory ensembles, which are composed of N_E and N_I neurons, respectively. (b) Schematic diagram that shows the reason why g_{sub}^E and g_{sub}^I are subtracted from g_{int} and g_{ext}, respectively, for $M = 2$. If two modules are synchronized with each other, the dynamics of the two modules are identical with those of one module with g_{int} and g_{ext}. Therefore, if appropriate values of g_{int} and g_{ext} are chosen, chaotic dynamics are expected to exist in the synchronized modules.

ensemble in the i-th module are defined as

$$T_{Ei} = (g_{int} - g_{sub}^E)I_{Ei} - g_{ext}I_{Ii} + \sum_{j=1}^{M} \epsilon_{ij}^E I_{Ej}, \quad (6)$$

$$T_{Ii} = (g_{ext} - g_{sub}^I)I_{Ei} - g_{int}I_{Ii} + \sum_{j=1}^{M} \epsilon_{ij}^I I_{Ej}, \quad (7)$$

where I_{Ei} and I_{Ii} are defined by Eq. (3), and they denote the synaptic inputs from the excitatory and inhibitory ensembles in an identical module, respectively. Note that the Fokker-Planck equations of M modules of the network can also be defined using Eqs. (6) and (7). The inter-module connection strengths ϵ_{ij}^E and ϵ_{ij}^I are defined using the modified Hebbian rule (Kanamaru & Okabe, 2000; Yoshioka & Shiino, 1998) defined as follows:

$$\epsilon_{ij}^E = \begin{cases} \epsilon_{EE}K_{ij} & \text{if } K_{ij} > 0 \\ 0 & \text{otherwise} \end{cases}, \quad (8)$$

$$\epsilon_{ij}^I = \epsilon_{IE}|K_{ij}|, \qquad (9)$$

$$K_{ij} = \frac{1}{Ma(1-a)} \sum_{\mu=1}^{p} \eta_i^\mu(\eta_j^\mu - a), \qquad (10)$$

where $\eta_i^\mu \in \{0,1\}$ are stored patterns with an average firing rate $a = 0.5$, p is the number of stored patterns, and ϵ_{EE} and ϵ_{IE} are parameters that scale connection strengths. When K_{ij} based on the modified Hebbian rule is positive, there exist both $E \to E$ and $E \to I$ inter-module connections, and such connections tend to facilitate inter-module synchronization. On the other hand, when $K_{ij} < 0$, there exist only $E \to I$ inter-module connections, and such connections tend to break inter-module synchronization.

Two additional parameters of regulation, g_{sub}^E and g_{sub}^I, are defined as $g_{sub}^E = \gamma\epsilon_{EE}$ and $g_{sub}^I = \gamma\epsilon_{IE}$ using a new parameter γ that is common to all modules. The purpose of introducing g_{sub}^E and g_{sub}^I is as follows. Let us consider a situation where only a single pattern is stored in the network, and the average behaviors of Ma ensembles that store the binary digit "1" in this pattern tend to synchronize with each other, namely, they satisfy $J_{Ei} = J_{Ej}$ and $J_{Ii} = J_{Ij}$ where i and j are arbitrary indices that store the binary digit "1". Such excitatory and inhibitory ensembles receive inputs with strengths $g_{int} + \epsilon_{EE}$ and $g_{ext} + \epsilon_{IE}$, respectively (see Fig. 2(a) and Eqs. (8), (9), and (10)). Thus, by subtracting ϵ_{EE} and ϵ_{IE} from g_{int} and g_{ext}, respectively, the dynamics of the one-module system with g_{int} and g_{ext} would also exist in this network composed of M modules. Such a situation is shown in Fig. 2(b). Therefore, the chaotic dynamics observed in a one-module system with g_{int} and g_{ext} would exist in the synchronized network. The inter-module synchronization of chaotic firings among two or three modules that have global connections was previously examined (Kanamaru, 2006). However, in the present network of M modules, the connections are not global but Hebbian; therefore, all of the Ma modules that store the binary digit "1" do not perfectly synchronize with each other because actually two or more patterns are stored in the network. Thus, $\gamma\epsilon_{EE}$ and $\gamma\epsilon_{IE}$ where $\gamma < 1$ are subtracted from g_{int} and g_{ext}, respectively, and γ is regulated to obtain maximal synchronization. Although the number M of modules can be arbitrarily chosen in principle, we set $M = 16$ and $p = 3$ in the following to reduce computational times. Moreover, the values of the parameters are fixed at $D = 0.0032$, $g_{int} = 4$, and $g_{ext} = 2.5$, which are identical with those used in Fig. 1(a). Three patterns $\eta_i^\mu (\mu = 1, 2, 3)$ are defined as

$$\eta_i^1 = \begin{cases} 1 & \text{if } i \le M/2 \\ 0 & \text{otherwise} \end{cases}, \qquad (11)$$

$$\eta_i^2 = \begin{cases} 1 & \text{if } M/4 < i \le 3M/4 \\ 0 & \text{otherwise} \end{cases}, \qquad (12)$$

$$\eta_i^3 = \begin{cases} 1 & \text{if } i \bmod 2 = 1 \\ 0 & \text{otherwise} \end{cases}. \qquad (13)$$

Under the above configurations, we analyze the dy-

namics of this network using the Fokker-Planck equations obtained in the limit of $N_E, N_I \to \infty$. Typical dynamics of the network with $\epsilon_{EE} = 1.2$ and $\gamma = 0.7$ are shown in Fig. 3. Note that J_{Ei} denotes the instan-
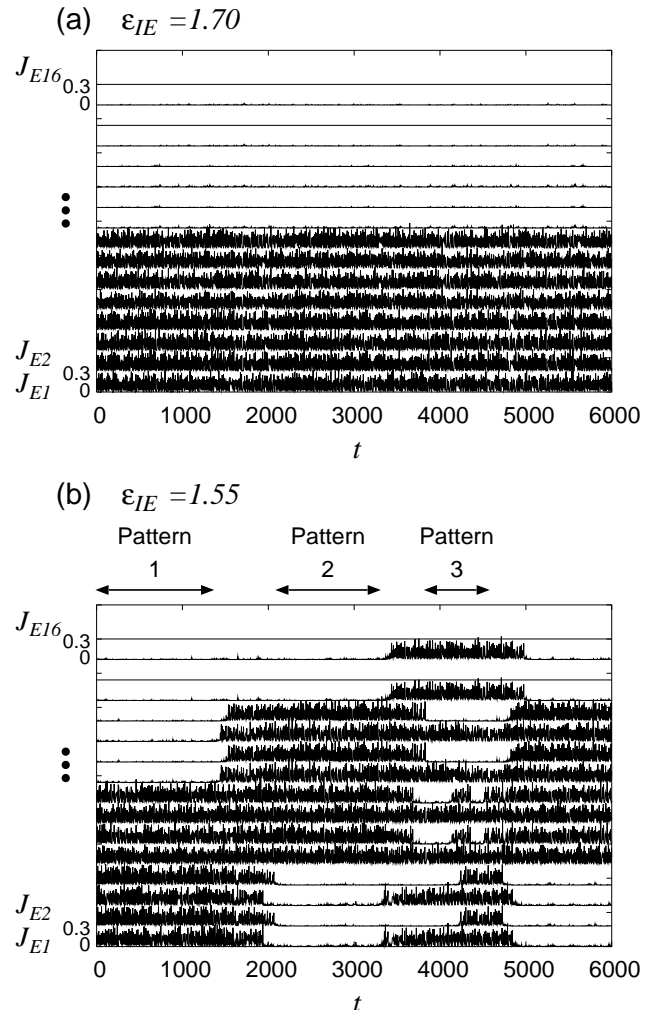

Figure 3: The dynamics of pattern retrieval in a network of 16 modules where $D = 0.0032$, $g_{int} = 4$, $g_{ext} = 2.5$, $\epsilon_{EE} = 1.2$, and $\gamma = 0.7$. (a) Successful retrieval of pattern 1 for $\epsilon_{IE} = 1.70$. (b) Chaotic pattern transitions for $\epsilon_{IE} = 1.55$. The instantaneous firing rates J_{Ei} of the excitatory ensembles are aligned so that they do not overlap.

taneous firing rate of the excitatory ensemble in the i-th module, and they are aligned so that they do not overlap. In Fig. 3(a), the dynamics of the network when pattern 1 is successfully retrieved for $\epsilon_{IE} = 1.70$ are shown. Figure 3(b) shows the chaotic pattern transitions for $\epsilon_{IE} = 1.55$, and it is observed that the retrieved pattern changes chaotically. To measure the distance between a set of firing rates J_{Ei} and the stored pattern η_j^μ, the overlap m^μ, which is similar to the inner product of two vectors, is defined in Appendix C. The change in overlap $m^\mu (\mu = 1, 2, 3)$ over time calculated from the

4

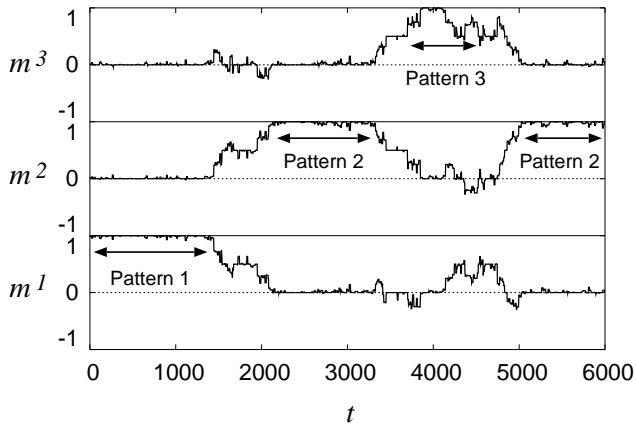data of Fig. 3(b) is shown in Fig. 4. It is observed that

Figure 4: Change in overlaps m^1, m^2, and m^3 over time calculated from the data in Fig. 3(b).

the overlap m^μ with pattern μ takes values close to 1 when pattern μ is retrieved, and it is also observed that the retrieved pattern changes chaotically.

The dependence of the time-average $\langle m^1 \rangle$ of overlap m^1 with pattern 1 on ϵ_{IE} is shown in Fig. 5. Note that
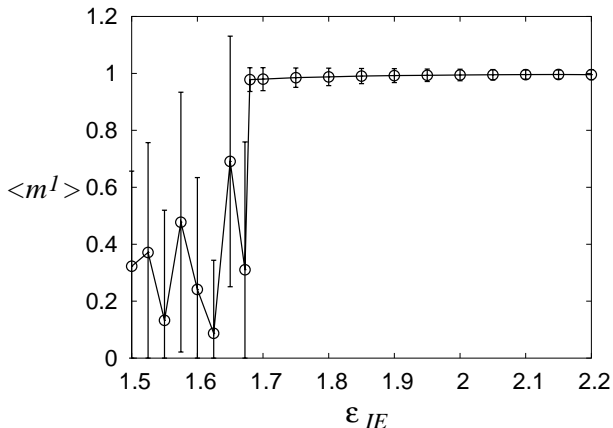

Figure 5: Dependence of the time-average $\langle m^1 \rangle$ of overlap m^1 with pattern 1 on ϵ_{IE}. The error bar denotes the standard deviation. Chaotic pattern transitions are observed for $\epsilon_{IE} < \epsilon_0 \sim 1.678$.

the initial state of the network was set so that pattern 1 is successfully retrieved. When $\langle m^1 \rangle$ takes values close to 1, the pattern-retrieval state is stable in the network. When $\epsilon_{IE} < \epsilon_0 \sim 1.678$, $\langle m^1 \rangle$ takes small values because of the chaotic pattern transitions. Three patterns are stored in this network; therefore, $\langle m^1 \rangle$ should be $1/3$, but it actually fluctuates widely because the number of data for time-averaging is finite. The properties of chaotic pattern transitions will be investigated in the next section.

The above analyses were performed using the canon-ical model of the slowly connected class 1 network, and similar results can be observed in the network composed of arbitrary class 1 neurons. The chaotic pattern transi-tions observed in the network of Morris-Lecar neurons (Ermentrout, 1996) with 3 patterns and 16 modules, each of which is composed of 1000 excitatory neurons and 1000 inhibitory neurons, are shown in Fig. 6. The
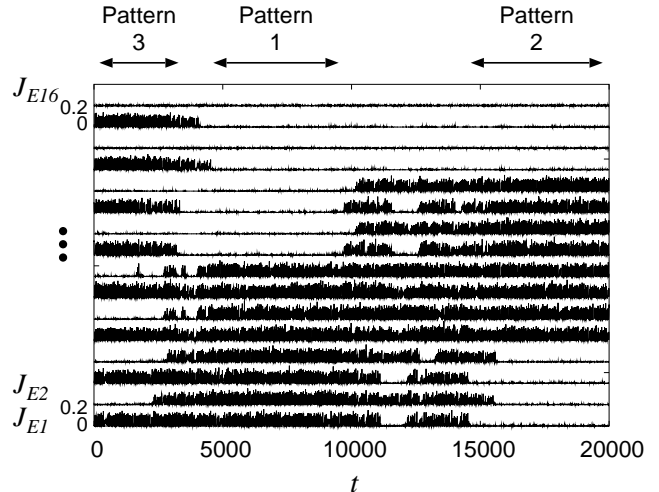

Figure 6: Chaotic pattern transitions observed in a net-work of Morris-Lecar neurons with 3 patterns and 16 modules, each of which is composed of 1000 excitatory neurons and 1000 inhibitory neurons. The values of the parameters are fixed at $D = 1.7 \times 10^{-5}$, $g_{int} = 0.3$, $g_{ext} = 0.1875$, $\epsilon_{EE} = 0.09$, $\epsilon_{IE} = 0.12$, and $\gamma = 0.7$. The ratio of ϵ_{EE} to g_{int} is 0.3, which is identical with the ratio in the canonical model in Fig. 3(b).

network of Morris-Lecar neurons is defined in Appendix D. Figure 6 shows that chaotic pattern transitions can also be observed in a network of Morris-Lecar neurons.

4 Properties of chaotic pattern transitions

In this section, detailed properties of chaotic pattern transitions are examined for values of ϵ_{IE} in three regions, namely, the bifurcation point where $\epsilon_{IE} = \epsilon_0 \sim 1.678$, the chaotic-pattern-transitions region where $\epsilon_{IE} < \epsilon_0$, and the stable-pattern-retrieval region where $\epsilon_{IE} > \epsilon_0$. All analyses in this section are performed us-ing the Fokker-Planck equations obtained in the limit of $N_E, N_I \to \infty$.

4.1 Mechanism of bifurcation

In this subsection, we consider the mechanism that gen-erates the chaotic pattern transitions at the bifurcation point $\epsilon_{IE} = \epsilon_0$.

5

First, let us examine the maximum value m_{max}^μ of overlap m^μ and its dependence on ϵ_{IE}. When $\epsilon_{IE} > \epsilon_0$, the pattern retrieval is stable; therefore, only m_{max}^1 takes the value 1, and m_{max}^2 and m_{max}^3 would take small values. When $\epsilon_{IE} < \epsilon_0$, all m_{max}^μ ($\mu = 1, 2, 3$) can take the value of 1. The dependence of m_{max}^μ on ϵ_{IE} is shown in Fig. 7, and it is observed that m_{max}^2 and m_{max}^3 can take the value 1 when $\epsilon_{IE} < \epsilon_0$. Note that m_{max}^2 or m_{max}^3
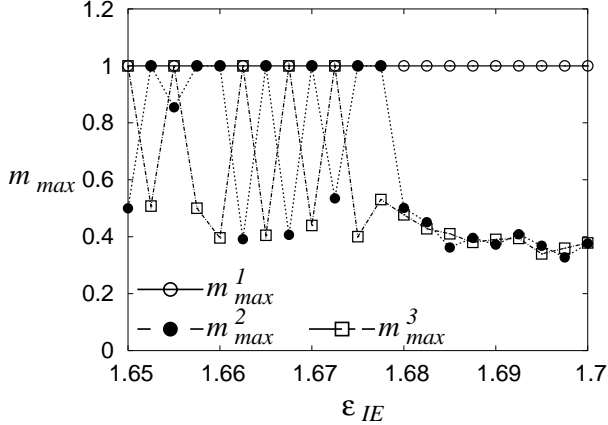

Figure 7: Dependence of the maximum value m_{max}^μ of overlap with pattern μ on ϵ_{IE}. For values of $\epsilon_{IE} < \epsilon_0 \sim 1.678$, all m_{max}^μ take the value of 1.

sometimes takes values smaller than 1 because the time length for simulations is finite. Moreover, it is observed that m_{max}^2 and m_{max}^3 take somewhat large values close to 0.5 even when $\epsilon_{IE} > \epsilon_0$. This is because m^μ, which fluctuates around 0, sometimes takes large values during short time intervals. The pattern transitions would take place when m_{max}^2 or m_{max}^3 exceeds a threshold, which is observed to be $m_{max}^\mu \sim 0.5$. Note that the state with overlap $m^\mu = 0.5$ is the mixed pattern of the stored pattern μ with another pattern. For example, the i-th component of the mixed pattern of patterns 1 and 2 is $\eta_i^1 \vee \eta_i^2$. In the following, such mixed patterns are denoted as the mixed pattern with $m^\mu = 0.5$. When the system happens to stay at the mixed pattern of patterns i and j, then the system can change its state to either pattern i or j. Therefore, when the fluctuating m^μ reaches $m^\mu = 0.5$, chaotic pattern transitions would take place.

4.2 Properties of chaotic pattern transitions

In this section, we explain the roles of the mixed pattern when chaotic pattern transitions take place. The previous subsection introduced the mixed pattern with $m^\mu = 0.5$. In our system, there is another mixed pattern with $m^\mu = 0.75$ whose components are $\eta_i^\mu \vee (\eta_i^\lambda \wedge \eta_i^\nu)$ or $\eta_i^\mu \vee (\eta_i^\lambda \wedge \bar{\eta}_i^\nu)$ ($\mu \neq \lambda, \lambda \neq \nu, \nu \neq \mu$). Let us note that the network switches its state from one pattern to another pattern via mixed patterns. For example, as shown in

Fig. 3(b), when the retrieved pattern changes from pattern 1 to pattern 2, the network stays at a mixed pattern $\eta^1 \vee \eta^2$ for $1500 < t < 2000$. At around $t \sim 4200$, pattern 3 with firings of J_{E6} and J_{E8} ($\eta^3 \vee (\eta^1 \wedge \eta^2)$) appears. Moreover, at around $t \sim 4500$, pattern 3 with firings of J_{E2} and J_{E4} ($\eta^3 \vee (\eta^1 \wedge \bar{\eta}^2)$) appears, and a mixed pattern $\eta^3 \vee \eta^1$ is also observed.

To understand chaotic pattern transitions, it is important to examine statistical properties of the system, such as the duration of pattern retrieval. To perform such analysis, it is required to separate the stored patterns, the mixed pattern with $m^\mu = 0.75$, and the mixed pattern with $m^\mu = 0.5$. Although we separated them by introducing an arbitrary threshold for m^μ, this separation did not give consistent results (data not shown). Thus, such analysis is for future study.

4.3 Properties of stable pattern retrieval

Even during the stable pattern retrieval shown in Fig. 3(a), there exist some instabilities caused by chaotic dynamics. Such instabilities are discussed in this subsection. First, the Lyapunov spectra (Ott, 1993) are numerically calculated by the method proposed by Nagashima & Baba (1999), and their dependence on the inter-module connection strength ϵ_{IE} is analyzed. To investigate the stability of a single pattern, we utilized the expansion rate for numerical calculation only when $m^\mu > 0.7$ where μ is the retrieved pattern. Because our model is a time-continuous system, there exists at least one spectrum that is zero when periodic or chaotic flows are stable, and we call this spectrum λ_0. The remaining spectra are called $\lambda_1, \lambda_2, \cdots$ in order of decreasing spectrum value in the following. The dependence of $\lambda_4, \lambda_5, \cdots, \lambda_8$ on the inter-module connection strength ϵ_{IE} are shown in Fig. 8. $\lambda_1, \lambda_2,$ and λ_3 are always
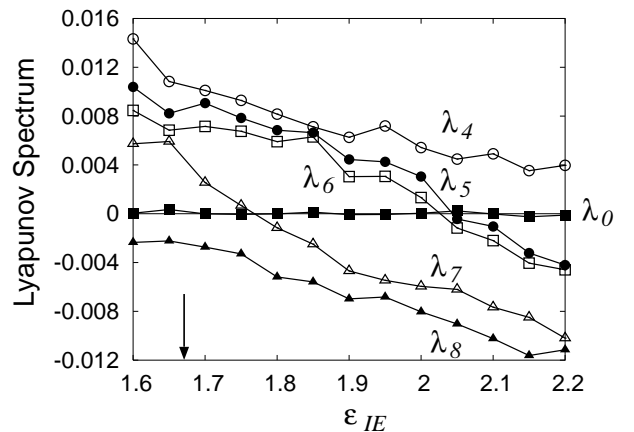

Figure 8: Dependence of $\lambda_4, \lambda_5, \cdots, \lambda_8$ on the inter-module connection strength ϵ_{IE}. The values of the parameters are set as $D = 0.0032$, $g_{int} = 4$, $g_{ext} = 2.5$, $\epsilon_{EE} = 1.2$, and $\gamma = 0.7$. Calculations were performed only when $m^\mu > 0.7$.

larger than λ_i $(i \geq 4)$ and their signs do not change in this parameter range; therefore, the plots of λ_1, λ_2, and λ_3 are omitted in Fig. 8 to clearly show the variations in λ_5, λ_6, and λ_7.

The transition from the successful pattern-retrieval state to the chaotic pattern-transition state takes place at $\epsilon_{IE} = \epsilon_0 \sim 1.678$ (Fig. 5), but the signs of the Lyapunov spectra do not change at that ϵ_{IE} (Fig. 8). Thus, it can be concluded that the emergence of the chaotic pattern transitions at $\epsilon_{IE} = \epsilon_0 \sim 1.678$ is not caused by the statistical instability of the retrieved pattern.

In the following, we explain why the signs of λ_5, λ_6, and λ_7 change as shown in Fig. 8. First, we consider the behaviors of modules $E1, E2, \cdots E8$ that show chaotic oscillations when pattern 1 is correctly retrieved as shown in Fig. 3(a). When ϵ_{IE} is large, for example, $\epsilon_{IE} = 2.2$, the relationships $J_{E1} = J_{E3}$, $J_{E2} = J_{E4}$, $J_{E5} = J_{E7}$, and $J_{E6} = J_{E8}$ hold, namely, these pairs of modules synchronize with each other in the sense that their instantaneous firing rates take identical values (data not shown). In this situation, eight modules show chaotic oscillations (see Fig. 3(a)), and four conditions of instantaneous firing rates are given to the network; therefore, the number of degrees of freedom is $8 - 4 = 4$. Thus, for $\epsilon_{IE} = 2.2$, the number of positive Lyapunov exponents is four (λ_1, λ_2, λ_3, λ_4) as shown in Fig. 8. When the signs of the exponents λ_5 and λ_6 change from negative to positive, blowout bifurcation (Kanamaru, 2006; Ott & Sommerer, 1994) takes place, and two synchronizations, i.e., $J_{E1} = J_{E3}$ and $J_{E6} = J_{E8}$, are broken. Moreover, when the sign of λ_7 changes from negative to positive, the synchronization, $J_{E5} = J_{E7}$, is broken. For $\epsilon_{IE} = 1.7$, the changes in $J_{E1} - J_{E3}$, $J_{E5} - J_{E7}$, and $J_{E6} - J_{E8}$ over time calculated from the data used in Fig. 3(a) are shown in Fig. 9. Although the pattern shown in Fig. 3(a) is successfully retrieved, instability of on-off intermittency (Fujisaka & Yamada, 1986; Hata & Miyazaki, 1997; Heagy, Platt, & Hammel, 1994; Kanamaru, 2006; Ott & Sommerer, 1994) exists in the dynamics of the network as shown in Fig. 9, namely, there exist nearly synchronized states where $J_{Ei} \sim J_{Ej}$, and this synchronized state is sometimes broken by intermittent bursts.

The reason why pairs of modules synchronize with each other can be understood as follows. Note that three pairs of modules $(1,3)$, $(5,7)$, and $(6,8)$ have identical bits of patterns for three patterns. Thus, for these pairs of modules i and j, the relationship $\eta_i^\mu = \eta_j^\mu$ $(\mu = 1, 2, 3)$ holds (see Eqs. (11), (12), and (13)), and the equation $\epsilon_{ik}^X = \epsilon_{jk}^X$ $(X = E$ or $I)$ is satisfied. Thus, modules i and j receive identical inputs, and the two modules in each of the three pairs of modules, i.e., $(1,3)$, $(5,7)$, and $(6,8)$ tend to synchronize with each other.
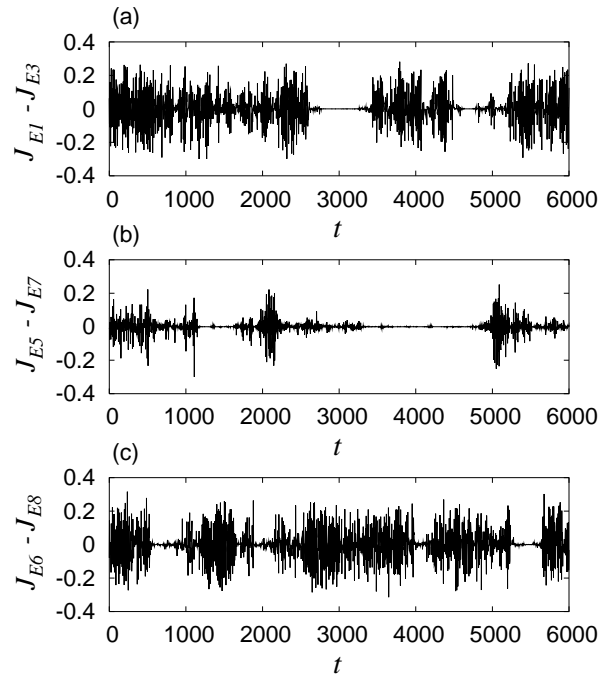

Figure 9: Changes in $J_{E1} - J_{E3}$, $J_{E5} - J_{E7}$, and $J_{E6} - J_{E8}$ over time calculated from the data used in Fig.3(a). The property of on-off intermittency is observed.

5 Discussion and conclusions

In models of associative memory composed of class 1 pulse neurons, we found chaotic pattern transitions where the pattern retrieved by the network changes chaotically. Because this network is based on the canonical model of slowly connected class 1 neurons (Izhikevich, 1999), it is theoretically guaranteed that the phenomena observed in this network can be observed in networks of any class 1 neurons. Accordingly, we found chaotic pattern transitions in a network of class 1 Morris-Lecar neurons. It was found that the mixed pattern of stored patterns plays an important role in chaotic pattern transitions. It was also found that several instabilities exist even when memory retrieval is stable.

In our model, chaos was generated by interactions in the network. However, we utilized this module of network as a single element of a model of associative memory. In this viewpoint, chaos is generated in an element of a model of associative memory. Thus, our model might be similar to the network of chaotic associative memory composed of chaotic neurons proposed by Adachi & Aihara (1997). Although their chaotic neurons are based on the conventional analog-valued neurons, our networks of chaotic associative memory were composed of pulse neurons.

As for the robustness of chaotic pattern transitions, it is known that chaos is widely observed in a one-module system (Kanamaru, 2006). To find chaotic pattern transitions, it is required to regulate the values of the inter-

module connection strengths ϵ_{EE} and ϵ_{IE}. Although the dependence of chaotic pattern transitions on ϵ_{EE} was not examined in the present study, we consider that chaotic pattern transitions would be robust because they were observed even in the network of finite number of Morris-Lecar neurons (see Fig. 6).

In our network, intra-module synchronization among neurons can be observed when a correct pattern is retrieved, although it is not perfect synchronization. This intra-module synchronization is similar to partial synchronization (van Vreeswijk, 1996) as shown in Fig. 1(c). As for inter-module synchronization, some pairs of modules show synchronization or on-off intermittency according to the strength of the inter-module connection. Even when pattern retrieval is successful, instability of on-off intermittency exists in the dynamics of the network as shown in Fig. 9. On the other hand, in pairs of modules that do not show synchronization nor on-off intermittency, there may be generalized synchronization (Rulkov, Sushchik, Tsimring, & Abarbanel, 1995) because there are deterministic relations among the dynamics of all modules, and its analysis is for future study.

The memory state can be regarded as an attractor of the system. Our network can exit from attractors using chaos, and, as a result, the pattern retrieved by the network changes chaotically. Note that the pattern transitions in associative memory can be realized not only by chaos but also by synchronized external inputs (Aoyagi & Aoki, 2004). Moreover, the phenomenon observed in Fig. 3(b) can be interpreted as a chaotic rearrangement of clusters of firing neurons, and such an interpretation might be related to the dynamical cell assembly hypothesis (Fujii et al., 1996; Hebb, 1949).

Acknowledgement

A Fokker-Planck equation of one-module system

To analyze the average dynamics of the one-module system, we use the Fokker-Planck equations (Gerstner & Kistler, 2002; Kuramoto, 1984) that are written as

$$\frac{\partial n_E}{\partial t} = -\frac{\partial}{\partial \theta_E}(A_E n_E)$$
$$+\frac{D}{2}\frac{\partial}{\partial \theta_E}\left\{B_E\frac{\partial}{\partial \theta_E}(B_E n_E)\right\}, \text{(A.1)}$$

$$\frac{\partial n_I}{\partial t} = -\frac{\partial}{\partial \theta_I}(A_I n_I)$$
$$+\frac{D}{2}\frac{\partial}{\partial \theta_I}\left\{B_I\frac{\partial}{\partial \theta_I}(B_I n_I)\right\}, \quad \text{(A.2)}$$

$$A_E(\theta_E,t) = (1-\cos\theta_E)+(1+\cos\theta_E)$$
$$\times(r_E+g_{EE}I_E(t)-g_{EI}I_I(t)),\text{(A.3)}$$
$$A_I(\theta_I,t) = (1-\cos\theta_I)+(1+\cos\theta_I)$$
$$\times(r_I+g_{IE}I_E(t)-g_{II}I_I(t)), \text{ (A.4)}$$
$$B_E(\theta_E,t) = 1+\cos\theta_E, \quad\quad\quad\text{(A.5)}$$
$$B_I(\theta_I,t) = 1+\cos\theta_I, \quad\quad\quad\text{(A.6)}$$

for the normalized number densities of excitatory and inhibitory ensembles, in which

$$n_E(\theta_E,t) \equiv \frac{1}{N_E}\sum\delta(\theta_E^{(i)}-\theta_E), \quad \text{(A.7)}$$

$$n_I(\theta_I,t) \equiv \frac{1}{N_I}\sum\delta(\theta_I^{(i)}-\theta_I), \quad \text{(A.8)}$$

in the limit of $N_E, N_I \to \infty$. The probability flux for each ensemble is defined as

$$J_E(\theta_E,t) = A_E n_E - \frac{D}{2}B_E\frac{\partial}{\partial \theta_E}(B_E n_E), \text{ (A.9)}$$

$$J_I(\theta_I,t) = A_I n_I - \frac{D}{2}B_I\frac{\partial}{\partial \theta_I}(B_I n_I), \quad \text{(A.10)}$$

respectively. The probability flux at $\theta = \pi$ can be interpreted as the instantaneous firing rate in this ensemble, and we denote it as $J_X(t) \equiv J_X(\pi,t)$ where $X = E$ or I.

$I_X(t)$ in Eq. (3) follows a differential equation that is written as

$$\dot{I_X}(t) = -\frac{1}{\kappa_X}\left(I_X(t) - \frac{1}{2}J_X(t)\right). \quad \text{(A.11)}$$

By integrating the Fokker-Planck equations (A.1) and (A.2) and the differential equation (A.11) simultaneously, the dynamics of the network that is governed by Eqs. (1) and (2) can be analyzed.

B Numerical integration of the Fokker-Planck equations

In this section, we provide a method of performing the numerical integration of the Fokker-Planck equations (A.1) and (A.2). Because the normalized number densities given by Eqs. (A.7) and (A.8) are 2π-periodic functions of θ_E and θ_I, respectively, they can be expanded as

$$n_E(\theta_E,t) = \frac{1}{2\pi}+\sum_{k=1}^{\infty}(a_k^E(t)\cos(k\theta_E)$$
$$+b_k^E(t)\sin(k\theta_E)),\text{ (B.1)}$$

$$n_I(\theta_I,t) = \frac{1}{2\pi}+\sum_{k=1}^{\infty}(a_k^I(t)\cos(k\theta_I)$$
$$+b_k^I(t)\sin(k\theta_I)), \text{ (B.2)}$$

and, by substituting them, Eqs. (A.1) and (A.2) are transformed into a set of ordinary differential equations

of a_k^X and b_k^X, which are written as

$$\frac{da_k^{(X)}}{dt} = -(r_X + \tilde{I}_X + 1)kb_k^{(X)}$$
$$-(r_X + \tilde{I}_X - 1)\frac{k}{2}(b_{k-1}^{(X)} + b_{k+1}^{(X)})$$
$$-\frac{Dk}{8}g(a_k^{(X)}), \qquad (B.3)$$

$$\frac{db_k^{(X)}}{dt} = (r_X + \tilde{I}_X + 1)ka_k^{(X)}$$
$$+(r_X + \tilde{I}_X - 1)\frac{k}{2}(a_{k-1}^{(X)} + a_{k+1}^{(X)})$$
$$-\frac{Dk}{8}g(b_k^{(X)}) \qquad (B.4)$$

$$g(x_k) = (k-1)x_{k-2} + 2(2k-1)x_{k-1} + 6kx_k$$
$$+2(2k+1)x_{k+1} + (k+1)x_{k+2}, \qquad (B.5)$$

$$\tilde{I}_E \equiv g_{EE}I_E - g_{EI}I_I, \qquad (B.6)$$
$$\tilde{I}_I \equiv g_{IE}I_E - g_{II}I_I, \qquad (B.7)$$
$$a_0^{(X)} \equiv \frac{1}{\pi}, \qquad (B.8)$$
$$b_0^{(X)} \equiv 0, \qquad (B.9)$$

where $X = E$ or I. Using a vector $\boldsymbol{x} = (I_E, I_I, a_1^E, b_1^E, a_1^I, b_1^I, a_2^E, b_2^E, a_2^I, b_2^I, \cdots)^t$, the ordinary differential equation $\dot{\boldsymbol{x}} = \boldsymbol{f}(\boldsymbol{x})$ is defined by (A.11), (B.3), and (B.4). By integrating this ordinary differential equation numerically, the time series of the probability fluxes J_E and J_I are obtained. For numerical calculations, each Fourier series is truncated at the first 40 or 60 terms.

C   Calculation of overlap

In this section, we provide a method of calculating the overlap m^μ between a set of instantaneous firing rates J_{Ei} of excitatory neurons in a module ($1 \leq i \leq M$) and the stored pattern η_i^μ.

Because J_{Ei} is an oscillating quantity, the overlap of the usual definition is also oscillating even when the correct pattern is retrieved. To obtain an overlap that maintains an almost constant value when the correct pattern is retrieved, we define a peak-value function $P_{Ei}(t)$ as $P_{Ei}(t) = J_{Ei}(t^*)$ where t^* is the nearest time point that gives a peak of $J_{Ei}(t)$ and satisfies $t^* < t$. Then we transform $P_{Ei}(t)$ to function $O_{Ei}(t)$ with a range of [0,1]:

$$O_{Ei}(t) = \begin{cases} 1 & \text{if } P_{Ei}(t) > \theta_2 \\ (P_{Ei}(t) - \theta_1)/(\theta_2 - \theta_1) & \text{if } \theta_1 \leq P_{Ei}(t) \leq \theta_2 \\ 0 & \text{if } P_{Ei}(t) < \theta_1 \end{cases}.$$
$$(C.1)$$

The $P_{E1}(t)$ and $O_{E1}(t)$ obtained from $J_{E1}(t)$ using $\theta_1 = 0.01$ and $\theta_2 = 0.1$ are shown in Fig. 10. Using $O_{Ei}(t)$, the overlap m^μ between the state of the network and the stored pattern η_i^μ is defined as

$$m^\mu = \frac{1}{Ma(1-a)}\sum_{i=1}^M (\eta_i^\mu - a)(O_{Ei} - a), \quad (C.2)$$

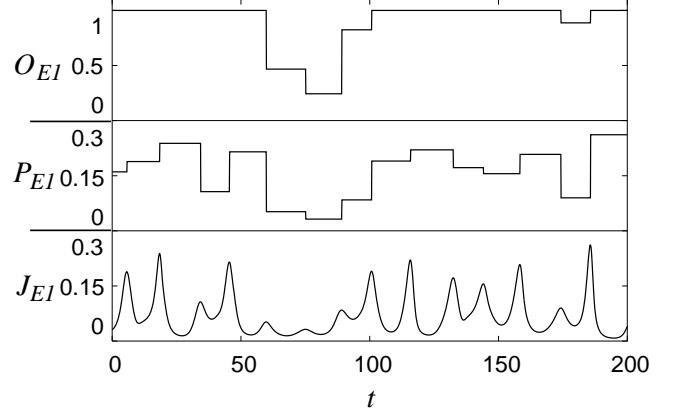Figure 10: Changes in $J_{E1}(t)$, $P_{E1}(t)$, and $O_{E1}(t)$ over time.

$$= \frac{1}{Ma(1-a)}\sum_{i=1}^M (\eta_i^\mu - a)O_{Ei}. \qquad (C.3)$$

D   The network of Morris-Lecar neurons

The dynamics of Morris-Lecar neurons in the excitatory and inhibitory ensembles are governed by two variables, (V_{Ek}, w_{Ek}) and (V_{Ik}, w_{Ik}), respectively, and they are written as

$$\dot{V}_{Ek}^{(i)} = -g_L(V_{Ek}^{(i)} - V_L) - g_K w_{Ek}^{(i)}(V_{Ek}^{(i)} - V_K)$$
$$-g_{Ca}m_\infty(V_{Ek}^{(i)})(V_{Ek}^{(i)} - V_{Ca})$$
$$+H_{Ek} + T_{Ek}(t) + \xi_{Ek}^{(i)}(t), \qquad (D.1)$$

$$\dot{w}_{Ek}^{(i)} = \lambda(V_{Ek}^{(i)})(w_\infty(V_{Ek}^{(i)}) - w_{Ek}^{(i)}), \qquad (D.2)$$

$$\dot{V}_{Ik}^{(i)} = -g_L(V_{Ik}^{(i)} - V_L) - g_K w_{Ik}^{(i)}(V_{Ik}^{(i)} - V_K)$$
$$-g_{Ca}m_\infty(V_{Ik}^{(i)})(V_{Ik}^{(i)} - V_{Ca})$$
$$+H_{Ik} + T_{Ik}(t) + \xi_{Ik}^{(i)}(t), \qquad (D.3)$$

$$\dot{w}_{Ik}^{(i)} = \lambda(V_{Ik}^{(i)})(w_\infty(V_{Ik}^{(i)}) - w_{Ik}^{(i)}), \qquad (D.4)$$

$$I_X(t) = \frac{1}{N_X}\sum_{j=1}^{N_X}\sum_k \frac{1}{\kappa_X}\exp\left(-\frac{t - t_k^{(j)}}{\kappa_X}\right)(D.5)$$

$$m_\infty(V) = 0.5(1 + \tanh((V - V_1)/V_2)), \qquad (D.6)$$

$$w_\infty(V) = 0.5(1 + \tanh((V - V_3)/V_4)), \qquad (D.7)$$

$$\lambda(V) = \frac{1}{3}\cosh((V - V_3)/(2V_4)), \qquad (D.8)$$

$$\langle \xi_X^{(i)}(t)\xi_Y^{(j)}(t')\rangle = D\delta_{XY}\delta_{ij}\delta(t - t'), \qquad (D.9)$$

$$X, Y = Ek \text{ or } Ik(k = 1, 2, \cdots, M), \qquad (D.10)$$

where the network is composed of M modules, the k-th module is composed of the excitatory ensemble Ek and the inhibitory ensemble Ik, H_{Ek} and H_{Ik} are external constant inputs to each ensemble, and the synaptic

9

inputs T_{Ek} and T_{Ik} are defined by Eqs. (6) and (7), respectively. The firing time of the i-th neuron in ensemble X is defined as the time at which $w_X^{(i)}$ crosses the value of 0.25 from lower values.

We choose values for the parameters that result in class 1 behavior, namely, $g_L = 0.5$, $g_K = 2$, $g_{Ca} = 1.33$, $V_L = -0.5$, $V_K = -0.7$, $V_{Ca} = 1$, $V_1 = -0.01$, $V_2 = 0.15$, $V_3 = 0.1$, $V_4 = 0.145$, and $\kappa_X = 7$. Using these values of the parameters, a saddle-node-on-limit-cycle bifurcation takes place when $H_{Ek}, H_{Ik} = H_0 \sim 0.0691$, and this neuron oscillates when $H_{Ek}, H_{Ik} > H_0$. In this work, H_{Ek} and H_{Ik} are fixed at $H_{Ek} = H_{Ik} = 0.068$; namely, all neurons without connections and noise stay at their equilibria. The values of the other parameters are fixed at $D = 1.7 \times 10^{-5}$, $g_{int} = 0.3$, $g_{ext} = 0.1875$, $\epsilon_{EE} = 0.09$, $\epsilon_{IE} = 0.12$, and $\gamma = 0.7$. Note that the values of $g_{ext}/g_{int} = 0.625$ and $\epsilon_{EE}/g_{int} = 0.3$ are identical with those used in the canonical model in Fig. 3(b).

The instantaneous firing rate $J_{Xk}(t)$ in ensemble X ($X = E$ or I) in the k-th module was calculated using the definition

$$ J_{Xk}(t) \equiv \frac{1}{N_{Xk}d} \sum_{i=1}^{N_{Xk}} \sum_j \Theta(t - t_j^{(i)}), \quad \text{(D.11)} $$

$$ \Theta(t) = \left\{ \begin{array}{ll} 1 & \text{if } 0 \le t < d \\ 0 & \text{otherwise} \end{array} \right. , \quad \text{(D.12)} $$

where $d = 1$.

References

[1] Adachi, M., & Aihara, K. (1997). Associative dynamics in a chaotic neural network. *Neural Networks*, *10*, 83–98.

[2] Aihara, K., Takabe, T., & Toyoda, M. (1990). Chaotic neural networks. *Physics Letters A*, *144*, 333–340.

[3] Aoyagi, T., & Aoki, T. (2004). Possible role of synchronous input spike trains in controlling the function of neural networks. *Neurocomputing*, *58-60*, 259–264.

[4] Ermentrout, B. (1996). Type I membranes, phase resetting curves, and synchrony. *Neural Computation*, *8*, 979–1001.

[5] Ermentrout, G. B., & Kopell, N. (1986). Parabolic bursting in an excitable system coupled with a slow oscillation. *SIAM Journal on Applied Mathematics*, *46*, 233–253.

[6] Feudel, U., Neiman, A., Pei, X., Wojtenek, W., Braun, H., Huber, M., & Moss, F. (2000). Homoclinic bifurcation in a Hodgkin-Huxley model of thermally sensitive neurons. *Chaos*, *10*, 231–239.

[7] Fujii, H., Ito, H., Aihara, K., Ichinose, N., & Tsukada, M. (1996). Dynamical cell assembly hypothesis – Theoretical possibility of spatio-temporal coding in the cortex. *Neural Networks*, *9*, 1303–1350.

[8] Fujisaka, H., & Yamada, T. (1986). Stability theory of synchronized motion in coupled-oscillator systems. IV. *Progress of Theoretical Physics*, *75*, 1087–1104.

[9] Gerstner, W., & Kistler, W. (2002). *Spiking Neuron Models*. Cambridge Univ. Press, Cambridge.

[10] Gilbert, C. D., & Wiesel, T. N. (1983). Clustered intrinsic connections in cat visual cortex. *Journal of Neuroscience*, *3*, 1116–1133.

[11] Gutkin, B. S., & Ermentrout, G. B. (1998). Dynamics of membrane excitability determine interspike interval variability: A link between spike generation mechanisms and cortical spike train statistics. *Neural Computation*, *10*, 1047–1065.

[12] Hata, H., & Miyazaki, S. (1997). Exactly solvable maps of on-off intermittency. *Physical Review E*, *55*, 5311–5314.

[13] Heagy, J. F., Platt, N., & Hammel, S. M. (1994). Characterization of on-off intermittency. *Physical Review E*, *49*, 1140–1150.

[14] Hebb, D. O. (1949). *The Organization of Behavior – a neuropsychological theory*. John Wiley, New York.

[15] Inoue, M., & Nagayoshi, A. (1991). A chaos neurocomputer. *Physics Letters A*, *158*, 373–376.

[16] Izhikevich, E. M. (1999). Class 1 neural excitability, conventional synapses, weakly connected networks, and mathematical foundations of pulse-coupled models. *IEEE Transactions on Neural Networks*, *10*, 499–507.

[17] Izhikevich, E. M. (2000). Neural excitability, spiking and bursting. *International Journal of Bifurcation and Chaos*, *10*, 1171–1266.

[18] Kanamaru, T. (2006). Blowout bifurcation and on-off intermittency in pulse neural networks with multiple modules. *International Journal of Bifurcation and Chaos*, *16*, 3309–3321.

[19] Kanamaru, T., & Okabe, Y. (2000). Associative memory retrieval induced by fluctuations in a pulsed neural network. *Physical Review E*, *62*, 2629–2635.

[20] Kanamaru, T., & Sekine, M. (2005). Synchronized firings in the networks of class 1 excitable neurons with excitatory and inhibitory connections and their dependences on the forms of interactions. *Neural Computation*, *17*, 1315–1338.

[21] Kaneko, K., & Tsuda, I. (2000). *Complex Systems: Chaos and beyond, a constructive approach with applications in life sciences.* Springer-Verlag, Berlin.

[22] Klauder, J. R., & Petersen, W. P. (1985). Numerical integration of multiplicative-noise stochastic differential equations. *SIAM Journal on Numerical Analysis, 22,* 1153–1166.

[23] Kuramoto, Y. (1984). *Chemical oscillations, waves, and turbulence.* Springer, Berlin.

[24] Nagashima, H., & Baba, Y. (1999). *Introduction to Chaos.* Institute of Physics Publishing, Bristol.

[25] Nara, S., & Davis, P. (1992). Chaotic wandering and search in a cycle-memory neural network. *Progress of Theoretical Physics, 88,* 845–855.

[26] Ott, E. (1993). *Chaos in Dynamical Systems.* Cambridge University Press, New York.

[27] Ott, E., & Sommerer, J. C. (1994). Blowout bifurcations: the occurrence of riddled basins and on-off intermittency. *Physics Letters A, 188,* 39–47.

[28] Rulkov, N. F., Sushchik, M. M., Tsimring, L. S., & Abarbanel, H. D. I. (1995). Generalized synchronization of chaos in directionally coupled chaotic systems. *Physical Review E, 51,* 980–994.

[29] Torikai, H., & Saito, T. (2004). Synchronization phenomena in pulse-coupled networks driven by spike-train inputs. *IEEE Transactions on Neural Networks, 15,* 337–347.

[30] Ts'o, D. Y., Gilbert, C. D., & Wiesel, T. N. (1986). Relationships between horizontal interactions and functional architecture in cat striate cortex as revealed by cross-correlation analysis. *Journal of Neuroscience, 6,* 1160–1170.

[31] Tsuda, I. (1992). Dynamic link of memory – Chaotic memory map in nonequilibrium neural networks. *Neural Networks, 5,* 313–326.

[32] Tsumoto, K., Yoshinaga, T., & Kawakami, H. (2002). Bifurcations of synchronized responses in synaptically coupled Bonhöffer-van der Pol neurons. *Physical Review E, 65,* 036230.

[33] Uchiyama, S., & Fujisaka, H. (2004). Chaotic itinerancy in the oscillator neural network without Lyapunov functions. *Chaos, 14,* 699–706.

[34] Varona, P., Torres, J. J., Huerta, R., Abarbanel, H. D. I., & Rabinovich, M. I. (2001). Regularization mechanisms of spiking-bursting neurons. *Neural Networks, 14,* 865–875.

[35] van Vreeswijk, C. (1996). Partial synchronization in populations of pulse-coupled oscillators. *Physical Review E, 54,* 5522–5537.

[36] van Vreeswijk, C., & Sompolinsky, H. (1996). Chaos in neuronal networks with balanced excitatory and inhibitory activity. *Science, 274,* 1724–1726.

[37] Yoshioka, M. (2005). Chaos synchronization in gap-junction-coupled neurons. *Physical Review E, 71,* 065203(R).

[38] Yoshioka, M., & Shiino, M. (1998). Associative memory based on synchronized firing of spiking neurons with time-delayed interactions. *Physical Review E, 58,* 3628–3639.